On: 03 February 2015, At: 22:24
Publisher: Taylor & Francis
Informa Ltd Registered in England and Wales Registered Number: 1072954 Registered office: Mortimer House, 37-41 Mortimer Street, London W1T 3JH, UK

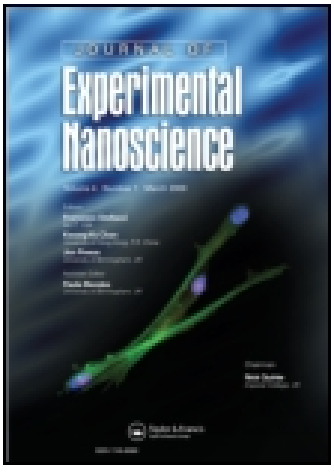

Journal of Experimental Nanoscience
Publication details, including instructions for authors and subscription information:
http://www.tandfonline.com/loi/tjen20

Synthesis and characterisation of microstructural α-Mn_2O_3 materials

Siddaramanna Ashoka [a], Pallellappa Chithaiah [a], Chikka Nagappa Tharamani [b] & Gujjarahalli Thimmanna Chandrappa [a]

[a] Department of Chemistry, Central College Campus, Bangalore University, Bangalore-560001, India

[b] Department of Chemistry, Ruhr Universität Bochum, Bochum, Germany

Published online: 07 Jul 2010.

To cite this article: Siddaramanna Ashoka, Pallellappa Chithaiah, Chikka Nagappa Tharamani & Gujjarahalli Thimmanna Chandrappa (2010) Synthesis and characterisation of microstructural α-Mn_2O_3 materials, Journal of Experimental Nanoscience, 5:4, 285-293, DOI: 10.1080/17458080903495003

To link to this article: http://dx.doi.org/10.1080/17458080903495003

Journal of Experimental Nanoscience
Vol. 5, No. 4, August 2010, 285–293

Taylor & Francis
Taylor & Francis Group

Synthesis and characterisation of microstructural α-Mn_2O_3 materials

Siddaramanna Ashoka[a], Pallellappa Chithaiah[a], Chikka Nagappa Tharamani[b] and Gujjarahalli Thimmanna Chandrappa[a]*

[a]*Department of Chemistry, Central College Campus, Bangalore University, Bangalore-560001, India;* [b]*Department of Chemistry, Ruhr Universität Bochum, Bochum, Germany*

(*Received 8 May 2009; final version received 16 November 2009*)

Low-dimensional α-Mn_2O_3 materials with novel surface morphologies have been prepared by thermal decomposition of hydrothermal-derived $MnCO_3$. The powder X-ray diffraction pattern reveals that the Mn_2O_3 microstructures are of cubic phase structure. From Fourier transform infrared spectroscopy results, the peaks around 600–450 cm^{-1} correspond to Mn–O bending vibrations. From the TGA results, the observed major weight loss ~31% between 350 and 540°C is due to the decomposition of $MnCO_3$ into Mn_2O_3. The X-ray photoelectron spectroscopy results showed that Mn is in +3 oxidation state. The peaks at 641.2 and 652.73 eV are assigned to the $Mn2p_{3/2}$ and $Mn2p_{1/2}$ of Mn^{+3} states, respectively. The scanning electron microscope images showed that the α-Mn_2O_3 products exhibit spheres, dumbbell- and peanut-shaped microstructure. These microstructures are mainly composed of wires/rods and particles. The scanning electron microscope results also revealed that the obtained α-Mn_2O_3 maintains the frame structure of the precursor $MnCO_3$.

Keywords: surface morphology; manganese oxide; hydrothermal; quinol

1. Introduction

Transition metal oxides nano/micro structures represent a broad class of materials that have been researched extensively due to their interesting catalytic, electronic and magnetic properties and wide scope of potential applications, such as magnetic resonance imaging (MRI) [1], solar cells [2] and heterogeneous catalysis [3,4]. There has been extensive recent research into fabrication and control of micro and nanostructural materials with novel morphologies because of their shape-dependent properties that these materials exhibit and the novel ways in which they can be applied [5,6]. Various techniques, including capping agents and templates, have been employed to accomplish this morphology control. However, these techniques are complex and often require further purification to remove the controlling agents, which may be introduced into the synthesis system and increase the production cost [5,6]. Therefore, developing the facile and template-free methods for shape and structure-controlled synthesis is of particular interest. Recently, a number of nano/micro structural metal oxides have been prepared using various organic reducing agents,

*Corresponding author. Email: gtchandrappa@yahoo.co.in

ISSN 1745–8080 print/ISSN 1745–8099 online

DOI: 10.1080/17458080903495003
http://www.informaworld.com

such as ethyl alcohol and oxalic acid via hydrothermal technique [7,8]. Hydrothermal method has been used to generate a wide range of materials with specific shapes, such as semiconductor nanowires and nanorods, transition metal oxide hollow spheres, multipods and so on. The hydrothermal method has been proved to be a useful method to prepare materials with novel morphologies and unusual properties.

Polymorphs of Mn_2O_3 have been proposed as cheap, environmental friendly catalysts for removing carbon monoxide and nitrogen oxide from waste gases [9,10] or as an oxygen storage component (OSC) for a three-way catalyst [11]. Moreover, Mn_2O_3 can also be used for preparing soft magnetic materials such as manganese zinc ferrite [12]. In the last decade, considerable attention has been focused on lithiation of Mn_2O_3 for intercalation compounds of Li–Mn–O as electrode materials for rechargeable lithium batteries [13,14]. Nanometer-sized Mn_2O_3 with remarkably increased surface area and greatly reduced size are expected to display better performance in all the above-mentioned applications [15]. For instance, a much larger surface-to-volume ratio can surely improve the catalysis capacity of Mn_2O_3 particles due to more adsorption of oxygen for oxidation of carbon monoxide and nitrogen oxides.

Mn_2O_3 has been synthesised in a variety of different morphologies including rods, wires and cubes, and conventionally, synthesised Mn_2O_3 materials have either wirelike or rodlike [16–18] morphology. However, there is little evidence of morphological control in these syntheses with the shapes of final products being dictated to a great extent by those of the precursors. Over the past two decades, several methods have been developed for the preparation of nano/micro structural Mn_2O_3. They include hydrothermal/solvothermal [19,20], hydrothermal reduction [21], thermal decomposition [22] and so on. In the solution-based synthesis, the formation of low-dimensional manganese oxide is usually dependent on the reductants. In the present contribution, we report a simple and facile method to synthesise α-Mn_2O_3 materials with novel surface morphology via thermal decomposition of $MnCO_3$ precursor that is synthesised via hydrothermal route. The effect of precursor concentration, reaction time and temperature on the morphology of Mn_2O_3 is also investigated.

2. Experimental procedure

In this study, potassium permanganate, quinol and urea were obtained from Aldrich Chemical Co. (Milwaukee, WI) and used as starting chemicals without any further purification. Crystalline manganese carbonate materials have been prepared by hydrothermal method. In a typical synthesis, 0.158 g $KMnO_4$ was dissolved in 20 ml (0.02 mM/L) distilled water under constant stirring. To this solution, 0.055–0.99 g of quinol dissolved in 20 ml (0.01–1.8 mM/L) of water was added. The reaction mixture was stirred for 20 min to obtain a homogeneous clear solution. The as-formed brown-coloured clear solution was transferred into 40-ml Teflon-lined stainless steel autoclaves (75 %), sealed and maintained at temperatures, 120–200°C for 2–5 days under autogenous pressure. After the hydrothermal process, the autoclaves were cooled to room temperature naturally, and the solid product was isolated from the solution by centrifugation. Then, the product was washed with distilled water followed by ethanol to remove the ions possibly remaining in the final product and dried in air. Finally, α-Mn_2O_3 product was obtained by thermal treatment of the as-prepared $MnCO_3$ precursor at 600°C for 1 h.

Powder X-ray diffraction data were recorded on Philips X'pert PRO X-ray diffractometer with graphite-monochromatised Cu-Kα radiation ($\lambda = 1.541$ Å) with Ni filter. The Fourier transform infrared (FTIR) spectrum of the sample was collected using Thermo Nicollet FTIR spectrometer. Thermal gravimetric analysis (TGA) was carried out using Perkins Elmer 7 series thermal analysis system at a heating rate of 5°C/min. The X-ray photoelectron spectroscopy (XPS) measurements of the α-Mn_2O_3 was carried out in an ultra-high vacuum (UHV) setup, equipped with a high-resolution Gammadata-Scienta SES 2002 analyser using Al-Kα X-ray source (1486.3 eV; anode operating at 14.5 kV and 50 mA). The scanning electron micrograph images were taken with JEOL (JSM – 840 A) scanning electron microscope equipped with an energy dispersive X-ray spectrometer.

3. Results and discussion

Figure 1 shows the PXRD patterns of the as-prepared $MnCO_3$ spherules (Figure 1(a)) and the resulting product (Figure 1(b)) through the thermal treatment at 600°C for 1 h. All the reflections of the PXRD pattern in Figure 1(a) can be readily indexed to pure hexagonal phase of $MnCO_3$ according to reported data (JCPDS Card No. 86-0173). All the peaks in Figure 1(b) can be indexed to the cubic structure of α-Mn_2O_3, corresponding to that of JCPDS Card No. 78-390. The broadening peaks in the PXRD pattern are mainly caused by the small average grain size of the as-obtained products. The PXRD results indicate that the thermal treatment temperature has a significant influence on the phase composition of product.

The formation of $MnCO_3$ and α-Mn_2O_3 was further confirmed by FTIR studies (Figure 2). From the Figure 2(a), the bands around 1400, 850 and 718 cm^{-1} are the characteristic vibration band of CO_3^{2-}. From the Figure 2(b), the absence of peak at 1400, 850 and 718 cm^{-1} indicates the complete conversion of manganese carbonate into manganese oxide. The peaks around 600–450 cm^{-1} correspond to Mn–O bending vibrations [23].

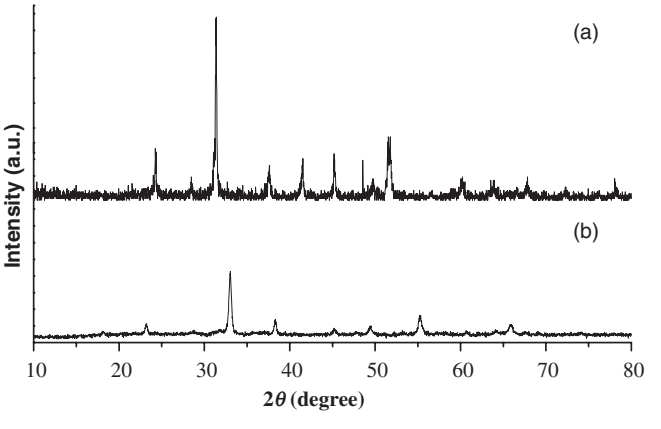

Figure 1. Powder X-ray diffraction patterns of (a) $MnCO_3$ and (b) α-Mn_2O_3 products.

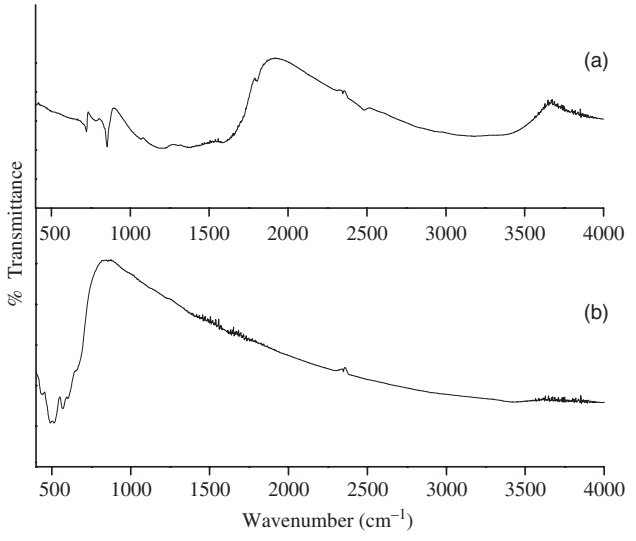

Figure 2. FTIR spectra of (a) $MnCO_3$ and (b) α-Mn_2O_3 products.

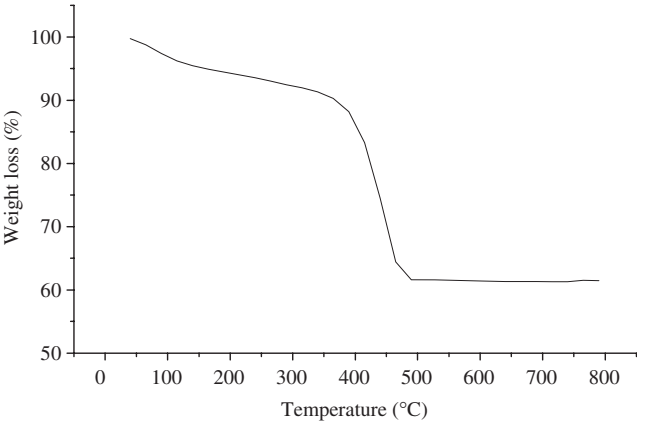

Figure 3. TGA curve of the $MnCO_3$ product.

The thermal behaviour of $MnCO_3$ product was investigated with TGA (Figure 3). The progressive weight loss in the TG curve at 40–350°C resulted from the removal of physically adsorbed water in the sample and the major weight loss happened between 350 and 540°C. The total weight loss was measured to be 31%, in good agreement with the theoretical value (31.3%) calculated from the following reaction [24]:

$$4MnCO_3 + O_2 \longrightarrow 2Mn_2O_3 + 4CO_2.$$

Figure 4(a) and (b) shows the XPS spectra of Mn (2p) and O (1s) core level regions of Mn_2O_3 product. Figure 4(a) shows that the Mn is in +3 oxidation state and the peaks at 641.2 and 652.73 eV corresponds to $Mn2p_{3/2}$ and $Mn2p_{1/2}$ of Mn^{3+} state, respectively.

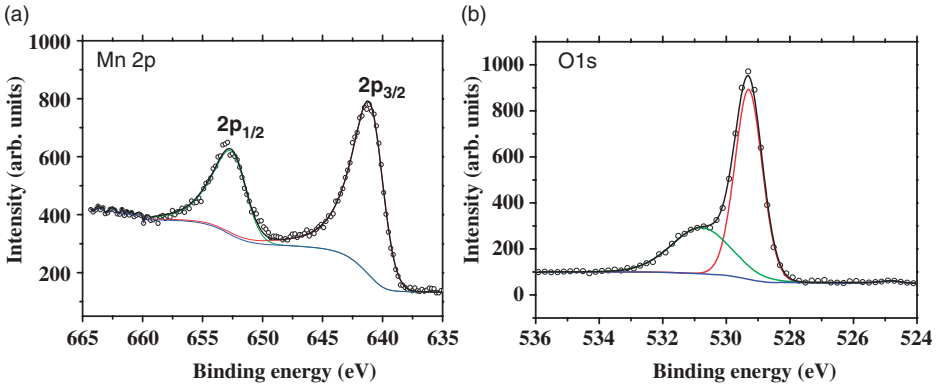

Figure 4. XPS spectra of (a) Mn-2p and (b) O-1s.

Figure 4(b) shows an intense peak at 529.30 along with a weak peak at 530.84 eV. The lower binding energy peak at 529.30 eV could be attributed to O^{2-} type of species associated with oxide of Mn, which is in the form of α-Mn_2O_3 [25].

The influences of the concentration of quinol on the morphology of the $MnCO_3$ have been investigated. Figure 5(a) presents the typical SEM image of $MnCO_3$ microstructures synthesised with 0.01 mM/L quinol at 200°C for 2 days. The products are composed of spherules and dumbbell-like morphologies with an even size distribution of a diameter of about 9–10 μm. These spherules and dumbbell morphologies are made up of particles/pins with good symmetry. The concentration of quinol plays an important role in controlling the morphologies of $MnCO_3$ materials. As the concentration of quinol increases to 0.02 mM/L, the products are made up of large amount of one-dimensional rod which is shown in inset of Figure 5(b). Further increase in the concentration of quinol to 0.06 mM/L, the products mainly contain spheres (Figure 5(c)) with almost smooth surfaces and the diameters of these spheres are found to be 11–16 μm. Figure 5(d) shows the typical SEM image of the $MnCO_3$ microspheres synthesised with 1.8 mM/L quinol. It is found that the products are mainly composed of dandelion-like microspheres with diameters of about 15 μm.

Figure 6 shows the SEM image of the α-Mn_2O_3 obtained by the thermal decomposition of $MnCO_3$ spheres (Figure 5(c)) at 600°C for 1 h. The surface morphology of α-Mn_2O_3 is almost similar to that of parent $MnCO_3$ microsphere.

The influence of the reaction time on the growth of $MnCO_3$ products was investigated. Figure 7(a) and (b) shows the SEM images of hydrothermal-treated samples for 3 days and 5 days at 200°C. These SEM images resemble dumbbell- and peanut-shaped structures with symmetrical morphology. The dumbbell- and groundnut-shaped structures are composed of many $MnCO_3$ rods (shown in inset of Figure 7(a)). The $MnCO_3$ rods are grown at their ends resulting in the fabrication of flower-like morphology.

Figure 8(a) and (b) shows the morphology of α-Mn_2O_3 sample synthesised through the thermal decomposition of dumbbell- and peanut-shaped precursor $MnCO_3$ at 600°C for 1 h. It can be seen that after the thermal decomposition, the morphology of each α-Mn_2O_3 sample has no change compared to that of the corresponding precursor $MnCO_3$.

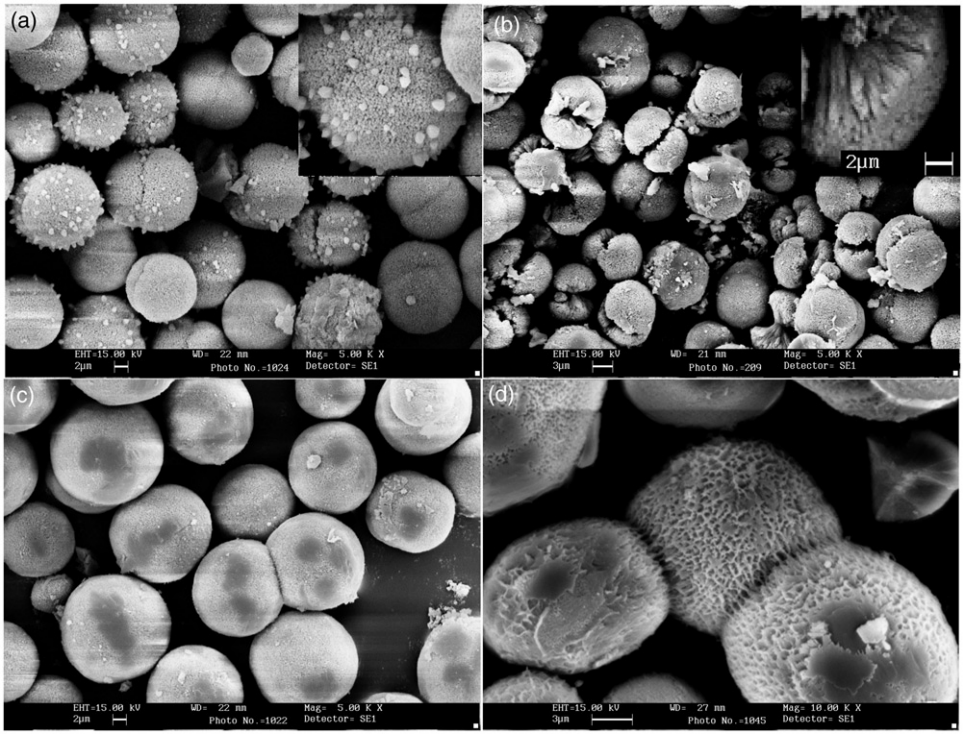

Figure 5. SEM images of $MnCO_3$ prepared at different concentrations of quinol (a) 0.01 mM/L, (b) 0.02 mM/L, (c) 0.06 mM/L and (d) 1.8 mM/L at 200°C for 2 days. Inset in 5(b) is a high magnified image.

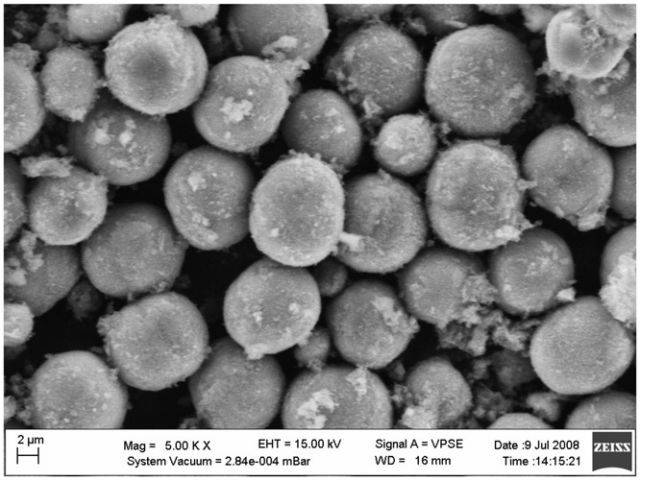

Figure 6. SEM images of α-Mn_2O_3 microsphere.

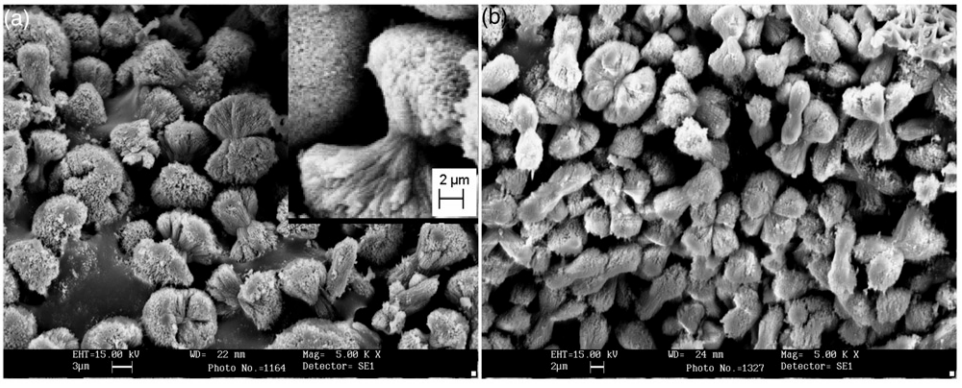

Figure 7. SEM images of $MnCO_3$ prepared at 200°C for (a) 3 days and (b) 5 days. Inset in 7(a) is a high magnified image.

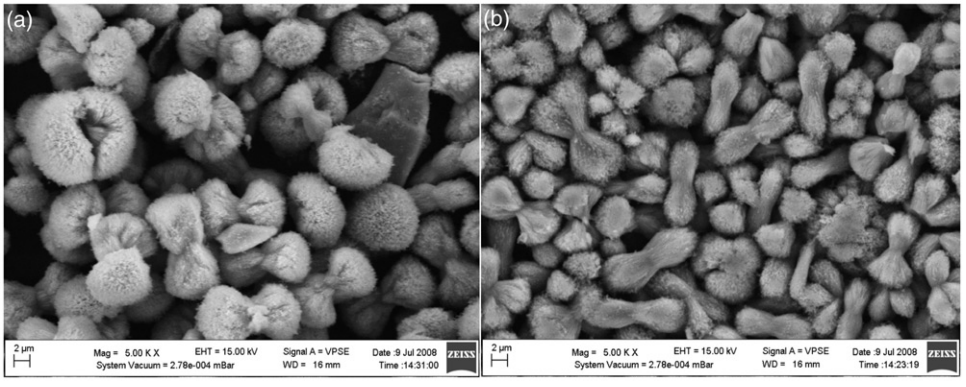

Figure 8. SEM images of α-Mn_2O_3 (a) dumbbell and (b) peanut structure.

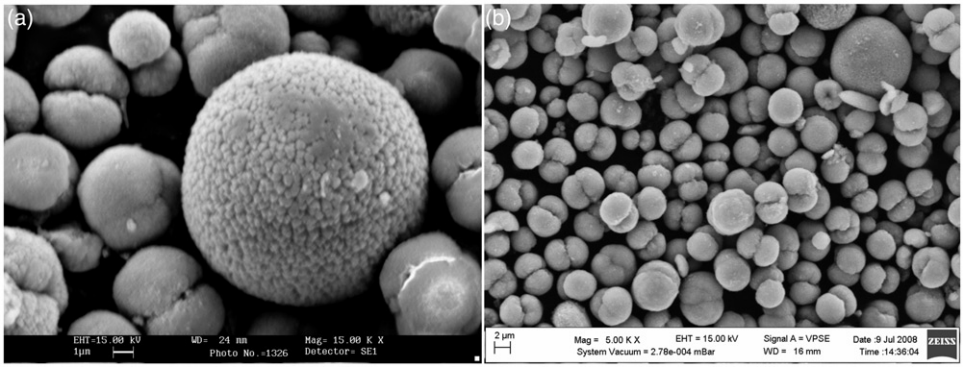

Figure 9. SEM images of (a) $MnCO_3$ prepared using 0.3 g urea at 200°C and corresponding (b) α-Mn_2O_3.

The sample prepared by adding 0.3 g urea to $KMnO_4$–quinol water system produces dumbbell and microspheres with nanoscaled, hole-shaped materials (Figure 9(a)). These nanoscaled holes are formed, maybe, due to the liberation of NH_3 gas from the decomposition of urea during hydrothermal. Figure 9(b) shows the morphology of α-Mn_2O_3 sample synthesised through the thermal decomposition of $MnCO_3$ dumbbell and microspheres precursor, indicating that the as-obtained α-Mn_2O_3 maintains the frame structure of the precursor.

The effect of temperature on α-Mn_2O_3 morphology is also investigated. The products prepared at 120 and 150°C show the similar morphology as observed in Figure 2(c).

4. Conclusions

In summary, we demonstrated a simple and facile method to the synthesis of low-valent, phase-pure α-Mn_2O_3 microstructure with novel surface morphologies via thermal decomposition of hydrothermal-derived $MnCO_3$. These Mn_2O_3 microstructures can be tuned to different shapes by adjusting the reductant concentration, reaction temperature and time. Further investigations might lead to an extension of this method to the preparation of other metal oxides with different morphologies.

Acknowledgements

G.T. Chandrappa is thankful to the Department of Science and Technology, NSTI Phase-IV, New Delhi, Government of India, for financial support to carry out the research work. We also thank Prof. Sarala Upadhya, Department of Mechanical Engineering, UVCE, Bangalore, for her help with SEM images.

References

[1] D.K. Kim, Y. Zhang, J. Kehr, T. Klason, B. Bjelke, and M. Muhammed, *Characterization and MRI study of surfactant-coated superparamagnetic nanoparticles administered into the rat brain*, J. Magn. Magn. Mater. 225 (2001), pp. 256–261.

[2] B. Oregan and M. Gratzel, *A low-cost, high-efficiency solar cell based on dye-sensitized colloidal TiO_2 films*, Nature 353 (1991), pp. 737–740.

[3] E.R. Stobbe, B.A. de Boer, and J.W. Geus, *The reduction and oxidation behavior of manganese oxide*, Catal. Today 47 (1999), pp. 161–167.

[4] M.I. Zaki, M.A. Hasan, and L. Pasupulety, *Influence of CuO_x additives on CO oxidation activity and related surface and bulk behaviours of Mn_2O_3, Cr_2O_3 and WO_3 catalysts*, Appl. Catal. A 198 (2000), pp. 247–251.

[5] Z. Zhang, J. Sui, L. Zhang, M. Wan, Y. Wei, and L. Yu, *Synthesis of polyaniline with a hollow, octahedral morphology by using a cuprous oxide template*, Adv. Mater. 17 (2005), pp. 2854–2857.

[6] S.M. Lee, Y.W. Jun, S.N. Cho, and J. Cheon, *Single-crystalline star-shaped nanocrystals and their evolution: Programming the geometry of nano-building blocks*, J. Am. Chem. Soc. 124 (2002), pp. 11244–11245.

[7] G. Nagaraju and G.T. Chandrappa, *Organic assisted hydrothermal route to MoO_2/HDA composite microspheres and their characterization*, Mater. Resc. Bull. 43 (2008), pp. 3297–3304.

[8] G. Li, K. Chao, H. Peng, K. Chem, and Z. Zhang, *Low-valent vanadium oxide nanostructures with controlled crystal structures and morphologies*, Inorg. Chem. 46 (2007), pp. 5787–5790.

[9] M. Baldi, V.S. Escribano, J.M.G. Amores, F. Milella, and G. Busca, *Characterization of manganese and iron oxides as combustion catalysts for propane and propene*, Appl. Catal. B Environ. 17 (1998), pp. L175–L182.
[10] H.M. Zhang, Y. Teraoka, and N. Yamazoe, *Effects of preparation methods on the methane combustion activity of supported Mn_2O_3 and $LaMnO_3$ catalysts*, Catal. Today 6 (1989), pp. 155–162.
[11] Y.F. Chang and J.G. McCarty, *Novel oxygen storage components for advanced catalysts for emission control in natural gas fueled vehicles*, Catal. Today 30 (1996), pp. 163–170.
[12] Chugai Electric Industrial Co. Ltd, Japan. Kokai Tokkyo Koho JP 02, 35, 915 [90, 35, 915] February 6, 1990.
[13] M. Tabuchi and K. Ado, *Synthesis of $LiMnO_2$ with α-$NaMnO_2$-type structure by a mixed-alkaline hydrothermal reaction*, J. Electrochem. Soc. 145 (1998), pp. L49–L52.
[14] T. Nakamura and A. Kajiyama, *Synthesis of Li–Mn spinel oxide using Mn_2O_3 particles*, Solid State Ionics 124 (1999), pp. 45–52.
[15] A. Zunger and S. Wagner, *New materials and structures for photovoltaics*, J. Electron. Mater. 22 (1993), pp. 3–16.
[16] T. Yamashita and A. Vannice, *NO decomposition over Mn_2O_3 and Mn_3O_4*, J. Catal. 163 (1996), pp. 158–168.
[17] H. Koyanaka, K. Takeuchi, and C.K. Loong, *Gold recovery from parts-per-trillion-level aqueous solutions by a nanostructured Mn_2O_3 adsorbent*, Sep. Purif. Technol. 43 (2005), pp. 9–15.
[18] W. He, Y. Zhang, X. Zhang, H. Yang, and H. Yan, *Low temperature preparation of nanocrystalline Mn_2O_3 via ethanol-thermal reduction of MnO_2*, J. Cryst. Growth 252 (2003), pp. 285–288.
[19] Y. Chen, Y. Zhang, Q.Z. Yao, G.T. Zhou, S. Fu, and H. Fan, *Formation of α-Mn_2O_3 nanorods via a hydrothermal-assisted cleavage-decomposition mechanism*, J. Solid State Chem. 180 (2007), pp. 1218–1223.
[20] W.N. Li, L. Zhang, S. Sithambaram, J. Yuan, X.F. Shen, M. Aindow, and S.L. Suib, *Shape evolution of single-crystalline Mn_2O_3 using a solvothermal approach*, J. Phys. Chem. C 111 (2007), p. 14694.
[21] S. Lei, K. Tang, Z. Fang, Q. Liu, and H. Zheng, *Preparation of α-Mn_2O_3 and MnO from thermal decomposition of $MnCO_3$ and control of morphology*, Mater. Lett. 60 (2006), pp. 53–56.
[22] N. Pinna, G. Garnweitner, M. Antonietti, and M. Niederberger, *A general nonaqueous route to binary metal oxide nanocrystals involving a C–C bond cleavage*, J. Am. Chem. Soc. 127 (2005), pp. 5608–5612.
[23] S.J. Parikh and J. Chorover, *FTIR spectroscopic study of biogenic Mn-oxide formation by pseudomonas putida GB-1*, J. Geomicrobiol. 22 (2005), pp. 207–218.
[24] L.X. Yang, Y.J. Zhu, H. Tong, and W.W. Wang, *Submicrocubes and highly oriented assemblies of $MnCO_3$ synthesized by ultrasound agitation method and their thermal transformation to nanoporous Mn_2O_3*, Ultrason. Sonochem. 14 (2007), pp. 259–265.
[25] J.F. Moulder, W.F. Stickle, P.E. Sobol, and K.D Bomben, *Handbook of X-ray Photoelectron Spectroscopy*, Perking-Elmer Corporation, Minnesota, USA, 1992.